Computers and Electronics in Agriculture xxx (xxxx) xxxx

Contents lists available at ScienceDirect

Computers and Electronics in Agriculture

journal homepage: www.elsevier.com/locate/compag

Automating field boundary delineation with multi-temporal Sentinel-2 imagery

Barry Watkins*, Adriaan Van Niekerk

Department of Geography and Environmental Studies, University of Stellenbosch, South Africa

ARTICLE INFO

Keywords:
Sentinel-2 imagery
Edge detection
Watershed segmentation
Object-based image analysis
Agricultural field boundary delineation

ABSTRACT

Knowledge of the extent and location of cultivated fields are critical for agricultural monitoring, food security planning and commodity trading. The increased observational capacity of remotely sensed data, such as Sentinel-2 imagery, constitutes a major advantage over in situ methods, particularly for agricultural applications that require frequent updates. However, the development of fully automated cultivated field delineation methods remains a challenge. In this study an existing object-based image analysis (OBIA) methodology, called Canny edge-detection in conjunction with watershed segmentation (CEWS), was modified to automatically identify and delineate agricultural fields from multi-temporal Sentinel-2 imagery in five diverse agricultural landscapes. The robustness of the technique was evaluated by comparing its outputs to those of standard per-pixel, supervised classifications. Reference field boundaries were manually digitised and used for quantitative accuracy assessments. Area and edge metrics were used to evaluate the accuracy of the extracted boundaries. Results show that, on average, CEWS produced significantly higher field boundary accuracies than the supervised per-pixel approach in terms of both mean absolute error (MAE) (~31 m lower) and overall accuracy (~13.8% higher). The closed field boundaries produced by CEWS, as well as its capability to operate without any a priori knowledge, was found to be its main strengths for integration into operational workflows. However, in complex landscapes (e.g. Swartland and Mooketsi) it was found that some fields had weak boundaries due to the homogeneity between adjacent fields, making edge detection problematic. The incorporation of higher resolution imagery into the edge detection process is proposed, particularly in agricultural areas with very small and irregularly shaped fields. Despite these challenges, it was concluded that the multi-temporal CEWS approach will perform well in most agricultural areas and is suitable for operational implementation.

1. Introduction

With the global population exceeding seven billion, food production has become a global concern (Fritz et al., 2015; Tollefson, 2012). Factors such as urban expansion and climate change are placing enormous pressure on agricultural land (Inglada et al., 2015). Conversely, agriculture is cited as one of the driving forces of climate change, contributing 30 – 35% to global greenhouse gas emissions. This poses a significant global challenge: to maintain food security while reducing the carbon footprint of agricultural activities (Karamura et al., 2013). Effective and responsive decisions on agricultural matters are needed to address these challenges simultaneously. It calls for the development of timely and accurate agricultural monitoring systems that can provide up-to-date insights into crop conditions, generate accurate estimations of crop yields and inform decision-making relating to hazards such as floods, droughts and civilian conflicts (Matton, Sepulcre Canto et al., 2015).

The extent and location of agricultural fields are fundamental data requirements of agricultural monitoring systems. Remote sensing (RS) techniques can provide datasets that cover extensive areas at high spatial and temporal resolution and are thus well suited for collecting agricultural data (Valero et al., 2016). However, remotely sensed imagery with high temporal resolution is critical as the seasonal patterns of agricultural fields are strongly related to the phenology of crops being grown (Atzberger 2013). Changes in the phenological stages of crops, which can happen within short periods, lead to changes in the spectral and structural properties of the crops. It has been shown that RS data acquired at short temporal intervals have the ability to capture crop properties throughout the growing season (Ozdogan et al., 2010; Pittman et al., 2010).

A number of techniques using low to high spatial resolution imagery have been developed to identify cultivated field extent (Matton,

* Corresponding author.
E-mail address: barrywatkins94@hotmail.co.za (B. Watkins).

https://doi.org/10.1016/j.compag.2019.105078
Received 4 June 2019; Received in revised form 24 October 2019; Accepted 29 October 2019
0168-1699/ © 2019 Elsevier B.V. All rights reserved.

Please cite this article as: Barry Watkins and Adriaan Van Niekerk, Computers and Electronics in Agriculture, https://doi.org/10.1016/j.compag.2019.105078

Sepulcre Canto et al., 2015). Low (250 m) resolution imagery provided by sensors such as MODIS have proved to be appropriate for quantifying cultivated extents (acreage) over very large areas (Lunetta et al., 2010; Pittman et al., 2010; Roumenina et al., 2015). However, such imagery is unsuitable for agricultural monitoring in heterogeneous landscapes where fields are smaller than the pixel size (Duveiller and Defourny 2010). Conversely, very high resolution (VHR) imagery provides finer detail and allows for more accurate delineation of individual cultivated fields but is often only available at low temporal frequency and can be expensive to acquire (Mueller et al., 2004). The recently launched Sentinel-2 satellite constellation can provide both relatively high spatial and temporal resolution imagery at no cost, thus offering a potential alternative to VHR imagery. Compared to Landsat-type sensors, the observational capacity of the Sentinel-2 satellite system offers significant improvements with its high number of spectral bands (13), five-day revisit time, 10 m – 60 m spatial resolutions and wide swath of 290 km. This allows for more timely estimates of crop extent, crop condition and crop type, which are fundamental indicators of a region's agricultural activities (Bontemps et al., 2015). From this perspective, the development of operational field boundary delineation methods that can be implemented for large areas and are transferable from one agricultural region to the next have become a priority (Matton, Canto et al., 2015).

A number of RS techniques to identify and delineate cultivated fields have been explored. The most commonly used technique is supervised classification (Peña et al., 2014). Supervised classification algorithms such as support vector machine (SVM) and random forest (RF) use in situ data, or a priori knowledge, to differentiate between crop type and land cover classes (Matton, Canto et al., 2015). However, the collection of in situ data is often expensive, time-consuming and prone to human error (Lucas et al., 2007). Furthermore, expert interaction is a prerequisite for successful implementation and consistent and accurate results (Thenkabail and Wu, 2012). An alternative is the knowledge-based approach, which uses expert knowledge to develop a sequence of rules for differentiating between classes. The main advantage of the knowledge-based approach is that the same model can potentially be used for multiple dates and regions. This makes it very attractive for operational systems as it can be fully automated. However, the creation of rules that are robust (i.e. will work in a variety of conditions) has been cited as the main limitation of a knowledge-based approach (Belgiu and Csillik, 2018).

Another differentiating aspect of cultivated field mapping methods relates to the spatial unit (minimum mapping unit) used in the classification step (Matton and Canto et al., 2015). Per-pixel classification assigns a class label to individual pixels based on their spectral signatures. However, this method does not take contextual information (surrounding the pixel of interest) into account, which tends to produce noisy maps (the so-called salt-and-pepper effect) (Blaschke et al., 2000; Schultz et al., 2015). In contrast to per-pixel techniques, object-based image analysis (OBIA) groups pixels based on a homogeneity criterion (Blaschke, 2010). Each object represents a homogenous region, and in the case of cultivated field mapping, individual fields are the objects of interest. In contrast to per-pixel classifications, entire objects are handled as minimum mapping units and are assigned labels according to a classification scheme (Lebourgeois et al., 2017). OBIA techniques often produce higher accuracies than per-pixel approaches (Belgiu and Csillik, 2018; Duro et al., 2012), but the implementation of transferable OBIA techniques for individual field boundary delineation remains a research gap (Yan and Roy, 2016).

Few examples of RS studies in which field boundaries were extracted exist. Those that are available have typically been carried out in small, localized areas or make use of visual interpretation to manually digitize field boundaries (Yan and Roy, 2016). A number of semi-automated techniques have been investigated, often involving either edge- or region-based methods (Ramadevi et al., 2010; Rydberg and Borgefors, 1999; Turker and Kok, 2013; Wuest and Zhang, 2009). Edge-based methods (or edge detection) focus on detecting object boundaries in an image. These boundaries are found by measuring the differences in grey level values between pixels (Kaganami and Beiji, 2009). Conversely, region-based methods group pixels together based on their grey level similarity (Li et al., 2010). Typical errors produced by edge-based techniques (e.g. gaps between edges) and region-based techniques (e.g. boundary errors) have limited their successful implementation for operational purposes (Chen et al., 2015; Fan et al., 2001). Hybrid methods that combine these techniques and exploit the strengths of each have consequently been proposed (Alemu, 2016; Butenuth et al., 2004; Li et al., 2010; Mueller et al., 2004; Rydberg and Borgefors, 2001). For instance, Li et al. (2010) proposed a hybrid approach to segment single-date Quickbird imagery in both an urban and agricultural landscape. Edge detection was performed to improve the positional accuracy of object borders and to emphasise weak edges. This was followed by a marker-based watershed algorithm to delineate the targeted object boundaries. A satisfactory boundary accuracy (78%) was achieved and the method reportedly performed well in reducing over-segmentation and retaining weak boundaries. In another hybrid approach, Chen et al. (2015) adopted a three-step strategy. First, the image was over-segmented into small objects. Second, the objects were merged in a global mutual best-fitting strategy using edge penalty and constrained spectral variance difference as merging criteria. The final step removed noise by merging very small objects with their nearest neighbour. The hybrid technique was quantitatively compared to a method based on the multi-resolution segmentation (MRS) algorithm using three measures, namely the rate of under-, over- and well-segmented objects. The hybrid method achieved a much higher rate of well-segmented objects (2.04/2.5) compared to MRS (1.07/2.5), highlighting its advantage over the traditional region-based approach. However, reliance on the manual selection of segmentation parameters was noted as a significant weakness of both approaches.

One limitation of the hybrid segmentation methods overviewed above is the use of single-date imagery. Delineating agricultural fields from such imagery can be challenging, as different crops can have similar spectral and structural characteristics during certain stages of the growing season (Esfahani, 2014). This is compounded when identical crops are planted on adjacent fields. Therefore, the acquisition of multi-temporal imagery throughout the growing season is necessary for consistent and accurate field boundary delineation. Watkins and Van Niekerk (2019) showed the advantage of using a multi-temporal OBIA approach for field boundary delineation. Edge detection was performed on multiple Sentinel-2 images in the Vaalharts irrigation scheme, South Africa. The multi-temporal edge layers were aggregated to enhance field edges while reducing within-field heterogeneity. Three segmentation algorithms, namely watershed, multi-resolution and multi-threshold, were compared for segmenting the aggregated edge layer. Canny edge-detection in conjunction with watershed segmentation (CEWS) was identified as the best method for mapping field boundaries (92.9%). The 10 m spatial resolution of the Sentinel-2 imagery was found to be too low for delineating small and irregular fields, but it produced satisfactory results in most cases. A major limitation of their study was that the evaluations were carried out in a single, relatively small area. No attempt was made to evaluate the robustness and transferability of the technique to other areas and in diverse agricultural systems (e.g. irrigated vs rain fed).

This article evaluates the robustness of the CEWS approach to identify and delineate agricultural fields using multi-temporal Sentinel-2 imagery. The methodology is evaluated in five study sites representing different climatic regions and agricultural practices, as well as a range of crop types. The paper also presents a number of proposed modifications to the CEWS technique to make it more transferable and robust. A per-pixel supervised classification was performed as a benchmark against which the CEWS approach was compared. The results are interpreted in the context of finding an operational solution for the identification and delineation of individual agricultural fields in

ARTICLE IN PRESS

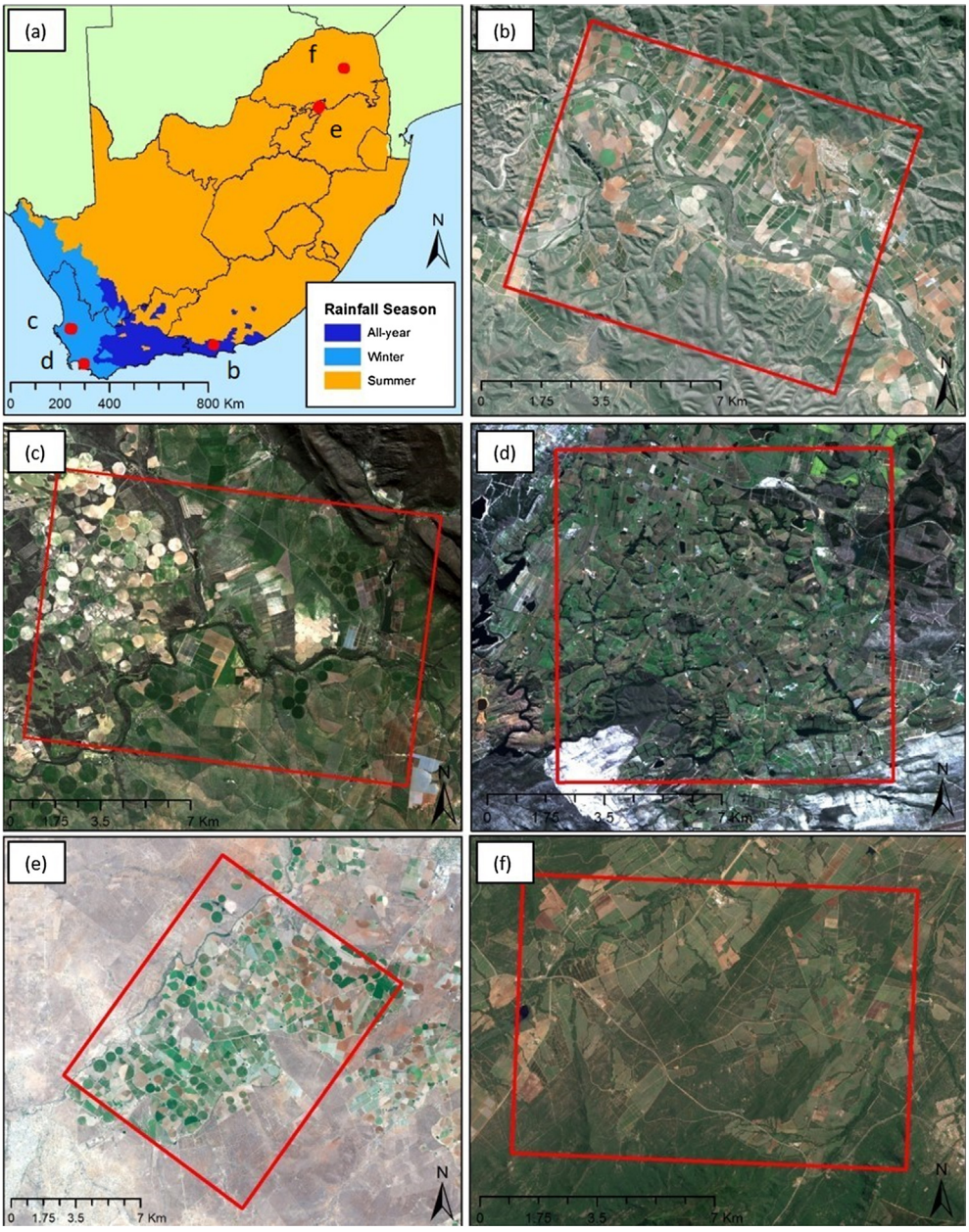

Fig. 1. (a) Location and extent of the five selected study sites in South Africa, (b) Patensie, (c) Swartland, (d) Grabouw, (e) Loskop, and (f) Mooketsi.

complex and dynamic agricultural landscapes.

2. Methods

2.1. Study area

Five study sites in South Africa, each with different environmental and agricultural conditions, were selected (Fig. 1). Two of the study areas (Swartland and Grabouw) have a Mediterranean climate (i.e. winter rainfall), two (Loskop and Mooketsi) receive rainfall predominantly during the summer and the fifth area (Patensie) receives rainfall throughout the year. These sites constitute a large variety of crops ranging from annuals (e.g. wheat, canola and tobacco) to perennial crops (e.g. vineyards and fruit trees). Irrigated and rain-fed crops were also represented, thus providing a large variation with which to test the robustness of the proposed methodology. Table 1 summarizes the chosen study areas.

2.1.1. Image collection

Multiple cloud-free Sentinel-2 images were acquired from April 2017 to April 2018. The imagery was acquired in Level-1C format, which is geometrically corrected and radiometrically calibrated to top of atmosphere (TOA) reflectance. Table 2 lists the number of cloud-free images used per study site.

2.2. CEWS workflow

2.2.1. Original CEWS workflow

The original CEWS workflow, developed by Watkins and Van Niekerk (2019), comprised five main processing steps:

1. Edge detection, executed on all individual images;
2. Aggregation of edge layers obtained in Step 1;
3. Image segmentation, performed on the aggregated edge layer created in Step 2;
4. Cultivated field extraction; and

Table 1
Summary of region characteristics for the five study sites.

Study site	Size	Rainfall regime	Mean annual rainfall	Common crops
Swartland	150 km^2	Winter	550 mm	Grapes, wheat and canola
Grabouw	100 km^2		950 mm	Horticulture and viticulture
Loskop	180 km^2	Summer	680 mm	Citrus, wheat, cotton, tobacco and groundnuts
Mooketsi	100 km^2		650 mm	Horticulture and wheat
Patensie	80 km^2	All-year round	487 mm	Citrus, tobacco and vegetables

Table 2
Number of cloud-free Sentinel-2 images per study area.

Study area	Number of image dates
Swartland	58
Patensie	24
Grabouw	20
Loskop	31
Mooketsi	19

5. Noise removal.

However, Watkins and Van Niekerk (2019) indicated that certain elements of this workflow might not be effective for application in multiple areas. For example, the watershed segmentation parameter was calculated using the Jenks natural breaks algorithm, which had to be manually adjusted. It is thus unlikely that the same parameter will work in all regions. This was confirmed when the original CEWS method was applied to the five selected sites. It was also noted that the rules used to differentiate crops from other land covers need to be adjusted to account for crop variations caused by environmental conditions. For instance, annual crops grown in the Loskop study site (summer rainfall regime) have different spectral signatures and temporal characteristics compared to the perennial crops (e.g. fruit trees and vineyards) grown in the Grabouw study site (winter rainfall regime). It was thus clear that the CEWS method would require modification for it to be transferable.

2.2.2. Modified CEWS workflow

Modifications were made to the original CEWS workflow to overcome some of the limitations described in the previous section. The objective of the modifications was to improve the transferability of the workflow so that it can be applied to diverse agricultural landscapes. The following subsections overview the alterations performed.

Step 1: Edge detection

Step 1 of the CEWS workflow required no major modifications, except that the Canny algorithm was implemented in Python using the Scikit-image Library (version 0.13.1). The red, blue, green and NIR bands were retained as input to the edge detection algorithm due to their higher (10 m) spatial resolution, which resulted in four edge images per Sentinel-2 image capture date (Table 2).

Step 2: Edge layer aggregation

The modified CEWS uses the mean value per pixel to aggregate the multi-temporal edge layers, which results in a single composite image per study area. The Z-score algorithm, followed by a linear scaling (from 0 to 1), was employed to standardize the composite edge layer and aid in the automation of the WS parameter selection (see next section).

Step 3: Image segmentation

CEWS makes use of the WS algorithm, as implemented in Trimble eCognition Developer 9, to segment the aggregated edge layer. As input, WS requires a height parameter for region merging. This parameter is used to compensate for the over-segmentation inherent in the WS algorithm and controls when adjacent objects can be merged (i.e. if an objects' maximum pixel value is below the specified height threshold). To make CEWS more robust, the Jenk's algorithm was substituted with a local thresholding procedure, as applied in the Scikit image Python package, to automatically find the most appropriate height threshold. The procedure applies a Gaussian filter to the aggregated edge image (in an 11 × 11-pixel window) and calculates the weighted mean per pixel, resulting in a generalized edge image. The height value is found by taking the standard deviation of the generalized image. Using this threshold in WS results in a set of image objects (segments) with boundaries coinciding with spectral transitions (edges).

Step 4: Cultivated field extraction

The original CEWS method employed a single rule-set to differentiate between actively cultivated fields and other land covers (non-cultivated). This was substituted by a rule-set per rainfall regime. The rule-sets were designed to be fully automated and reproducible, and replaces the commonly used supervised classification approach that requires a priori data. Based on the work by Huete (1988), Maselli and Rembold (2001), and Zheng et al. (2015), four normalized difference vegetation index (NDVI)-based features, namely maximum (max), minimum (min), range (ran) and standard deviation (std) were derived from the Sentinel-2 images acquired per area. These features were used as input for a classification and regression tree (CART) algorithm, as implemented in Salford Predictive Modeler software, to generate a decision tree, from which the values that best separate (classify) actively cultivated fields from other land uses could be determined. To train the CART algorithm, randomly sampled points (1 250) were generated and manually labelled (using visual interpretation) as either cultivated or non-cultivated fields.

Table 3 lists the rules per rainfall region. Image objects that did not satisfy the conditions of the rules were excluded from further consideration.

The all-year round and winter rainfall regions required one or two rules, while the summer rainfall region required five. A commonality among the regions is the use of the max NDVI feature. The summer rainfall region ruleset made use of three features, namely max, std and min NDVI.

Table 3
Rule sets per study area.

	Winter rainfall		All year rainfall	Summer rainfall	
Rule set	Swartland	Grabouw	Patensie	Loskop	Mooketsi
#1	min NDVI > 0.51 &std NDVI > 0.05		max NDVI > 0.63	max NDVI > 0.48 &min NDVI < = 0.17	
#2	–		–	max NDVI > 0.53 &min NDVI > 0.17 &std NDVI < = 0.12	

ARTICLE IN PRESS

Step 5: OBIA noise removal

Although the salt-and-pepper effect is not common in OBIA approaches, small irrelevant objects can occur. These can be the result of infrastructure (e.g. pivot irrigation) or small areas affected by salt accumulation or waterlogging. Therefore, a simple rule to identify and discard small objects, that are completely surrounded by cultivated areas, was employed in the final step (Step 5). The rule was identical to that of the original CEWS method.

2.3. Supervised per-pixel classification workflow for mapping cultivated areas

A semi-automated supervised per-pixel (PP) classification was performed to serve as a benchmark for the autonomous knowledge-based results. The RF algorithm was chosen for this purpose, as it has been shown to provide good accuracies for crop type differentiations (Belgiu and Csillik, 2018; Forkuor et al., 2017). Scikit-learn's RF package version 0.18.2 was used for the implementation. All features used by CEWS were used as input for the RF algorithm and trained with the identical sets of training samples used in the CART analysis (see Step 4 of the CEWS workflow). A majority filter (3 × 3 pixels) was used as a post classification step to remove some of the salt-and-pepper effect inherent in PP approaches (Quynh Trang et al., 2016). The subsequent raster classifications (cultivated vs. non-cultivated) were converted to a vector format. The resulting polygons thus represented contiguous areas covered by actively growing crops.

2.4. Accuracy assessment

Despite the popularity of image segmentation algorithms, methods to evaluate the effectiveness of a segmentation output remain elusive (Clinton et al., 2010; Meyer and Van Niekerk, 2015). Ideally, an image segmentation output should result in object delineations (boundaries) that match those of the targeted real-world features (e.g. agricultural fields). The most common causes of poor image segmentations are over-segmentation (OS), under-segmentation (US) and boundary offsets. OS occurs when the segmented objects are smaller than the target features, whereas US causes objects to be larger. Boundary offsets occur when there is a consistent spatial shift in the extracted boundaries.

No single accuracy measure can adequately assess the combined three types of segmentation errors (Weidner, 2008). While OS and US are commonly calculated using topological (area) relationships, boundary offsets are measured using geometrical (edge) metrics (Zhan et al., 2005). A number of area-based metrics have been proposed to calculate US and OS (Clinton et al., 2010; Möller et al., 2007; Weidner, 2008); however, these metrics do not evaluate the accuracy of the delineated object boundaries. Delves et al. (1992) proposed an edge metric that calculates the average distance error between reference boundaries and the extracted boundaries. This method has been shown to be successful in assessing the accuracy of segmented object boundaries (Meyer and Van Niekerk, 2015). A similar metric, namely the MAE distance metric, was applied in this study.

MAE calculates the Euclidean distance (ED) between the centres of two cells representing the extracted and reference boundary respectively (Fig. 2). To assess the accuracy of the extracted boundaries, two measures of MAE were calculated. MAE_i measures the distance from the centre of a reference boundary cell to the centre of the nearest extracted boundary cell, thereby providing an indication of how closely the extracted boundaries represent the reference boundaries in geographical space. Conversely, MAE_j measures the distance from each extracted boundary cell to the nearest reference boundary cell, thus providing an indication of boundaries within a field (i.e. providing an indication of OS). Both instances of MAE were calculated by the following formulae:

$$MAE_i = \frac{\sum EDi}{N} \quad (1)$$

where ED_i represents the ED measured from the centre of the reference cell to the centre of the extracted cell, while N is the total number of boundary cells in the reference dataset.

$$MAE_i = \frac{\sum EDj}{N} \quad (2)$$

where ED_j refers to the ED measured from the centre of the extracted cell to the centre of the reference cell. MAE_i and MAE_j were summed to get a sense of overall agreement between the extracted and reference boundaries, where low values indicate high agreement.

$$MAE = MAE_i + MAE_j \quad (3)$$

The blue arrows in Fig. 2b illustrate the increased distance calculated from the extracted field boundaries to the reference boundaries when OS occurs.

Reference field boundary datasets consisting of 100 active fields per study site were manually digitised using a combination of Sentinel-2 (10 m) imagery acquired from April 2017 to April 2018 and very high resolution (50 cm to 30 cm) satellite imagery from the ArcMap (version 10.4) base layer.

A confusion matrix approach was devised to calculate several area-based metrics. The matrix consisted of 10 000 samples, with 5 000 "boundary" samples selected randomly along the reference boundaries and another 5 000 "not-boundary" samples randomly selected more than 10 m away from the reference boundaries. The overall accuracy (OA), Kappa index (K), commission error (CE) and omission error (OE) were calculated from the confusion matrix. The OE quantifies the accuracy of the extracted boundaries along the reference boundaries, where a high value suggests that the extracted field boundaries were not delineated well. CE indicates false boundaries within a field, often due to OS. The McNemar's test was employed as an additional measure to test for significance of differences among accuracy measures, with p-values of 0.05 (or lower) regarded as significant.

3. Results

The results in Table 4 show that the two highest OAs (82.9% and 83.6%) of the CEWS methodology are recorded in the Patensie and Grabouw regions (Experiments 5 and 2). The lowest OA (61.3%) was obtained when the PP approach was applied in Mooketsi (Experiment 3). In addition, the PP approach also produced the second lowest OA (69%) in Swartland (Experiment 1). When OEs are considered, the CEWS scenarios recorded errors ranging from 27.1% to 38%. In contrast, the OEs for the PP scenarios are significantly ($p < 0.0001$) higher and range from 44.3% to 54%. Regarding CE, the CEWS scenarios in Experiments 4 and 5 (Loskop and Patensie) produced the lowest errors (1.3% and 1.4% respectively), and the highest CE (31.2%) was recorded by the PP scenario in Mooketsi (Experiment 3). CEWS recorded a significantly ($p < 0.0001$) higher mean OA (82.0%) than the OA (69%) of the PP approach. In addition, the lower standard deviation produced by the OBIA method for OA (1.4%) suggests a higher consistency. Similarly, the mean and standard deviation for the OE and CE of CEWS were lower (with the exception of the standard deviation for the OE).

Fig. 3 visually compares the CEWS and PP results in a detailed area in Patensie (Experiment 5). In this area, CEWS was 13% more accurate than the PP method. In addition, CEWS has the benefit of producing closed individual field boundaries while reducing the salt-and-pepper effect common in PP classification outputs. The red circles in Fig. 3b highlight some examples of this salt-and-pepper effect, whereas the red circles in Fig. 3c illustrate the closed field boundaries created by CEWS.

The edge-based metrics reveal that the field boundaries created by CEWS match the reference fields more closely than those produced by the PP method. The $MAEs_i$ for the CEWS scenarios show a low mean of

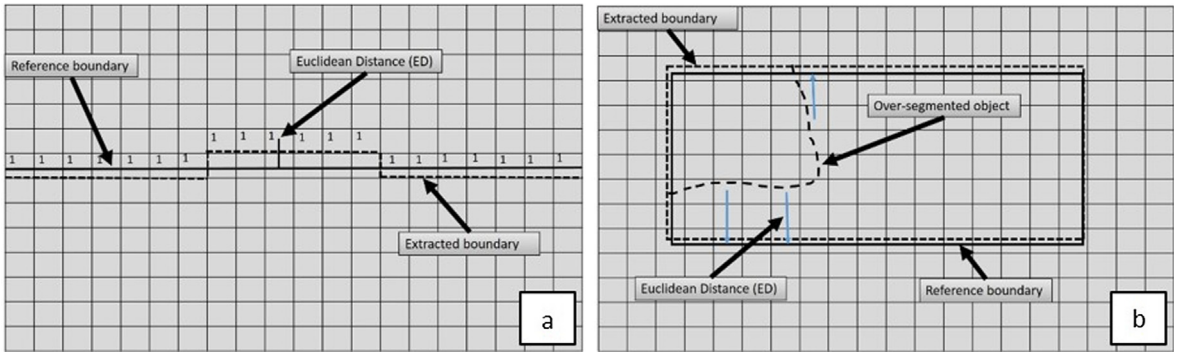

Fig. 2. Conceptual illustration of ED calculations, where (a) MAE_i depicts the accuracy along the boundary and (b) MAE_j represents the level of OS.

11.2 m (with the exception of Experiment 1, which recorded an MAE_i of 22.1 m). Generally, the $MAEs_i$ of the PP experiments are substantially higher, with a mean of 18.3 m. The 11.2 m mean MAE_i of CEWS is notable as it means that the technique produced field boundaries that are, on average, approximately one pixel (10 m) displaced from the reference boundaries. However, this low MAE_i comes at the cost of a slightly higher MAE_j, which suggests some level of OS. A similar observation is made for the PP scenarios. When the combined MAE is considered, it is clear that the CEWS boundaries are substantially more accurate than those generated by the PP approach.

Fig. 4 demonstrates the qualitative advantage of the automated CEWS approach. The red circles in Fig. 4b and Fig. 4c outline where the PP approach was unable to delineate individual fields (they are regarded as one field). In contrast, CEWS produces clear divisions between the fields.

Fig. 5 illustrates a limitation of both the CEWS and PP approaches. The techniques fail in areas with a high degree of homogeneity between adjacent fields (typical in areas such as Swartland and Mooketsi). The red circles in Fig. 5 indicate where the CEWS and PP experiments were unable to delineate the individual adjacent fields. However, the larger areas making up those individual fields were successfully identified and delineated. The agriculture in these regions comprise largely annual rain-fed crops (e.g. wheat, canola, medics). The blue circles indicate individual fields that were not successfully identified and delineated by CEWS. This contributed to the slightly larger combined MAE values obtained in Swartland (41.6 m) and Mooketsi (26.3 m) compared to Grabouw (14.7 m), Patensie (20.6 m) and Loskop (21.9 m).

Fig. 6 illustrates the inability of the Sentinel-2 (10 m) imagery to effectively delineate small and irregular fields in a detailed area of Grabouw (red circles). However, the high mean OA (83.6%) and low mean combined MAE (14.7 m) of the CEWS workflow suggests that it works well for most of the fields included in the reference set.

4. Discussion

Agricultural monitoring systems are becoming increasingly important in addressing challenges relating to climate change and food security. Accurate and up-to-date field boundary information is vital for developing efficient and effective agricultural monitoring systems, and the development of operational field boundary delineation methods have become a priority. An OBIA field boundary delineation procedure, originally developed by Watkins and Van Niekerk (2019), was modified in this study to make it more universally applicable. Firstly, the selection of the WS height parameter, which was originally manually selected from the output of the Jenks natural breaks algorithm, was substituted for an automated process using a thresholding method available in the Scikit image python package. Secondly, five study sites located throughout South Africa were selected to represent various environmental and agricultural regions. The sites were grouped into three different rainfall regimes and a knowledge-based rule-set was developed for each regime to eliminate non-cultivated areas from further consideration.

Results show that the modified CEWS approach produces superior results when compared to the conventional PP supervised classifications. CEWS produced objects with reduced within-field heterogeneity (salt-and-pepper effect) (Fig. 3b). This finding is in agreement with Belgiu and Csillik (2018) who compared PP and OBIA techniques to classify various crop types using multi-temporal Sentinel-2 imagery. They found that the OBIA techniques outperformed the PP approaches in three study sites. Another advantage of an OBIA approach is that individual cultivated fields are delineated with closed boundaries (Fig. 3c). Closed field boundaries provide a significant advantage and

Table 4
Area- and edge-based metric results.

				Area-based metrics				Edge-based metrics		
Rainfall regime	**Region**	**Experiment**	**Method**	**OA (%)**	**OE (%)**	**CE (%)**	**K**	**MAE_i (m)**	**MAE_j (m)**	**Combined MAE**
Winter	Swartland	Experiment 1	CEWS	82.0	31.4	2.5	0.7	22.1	19.5	41.6
			PP	69.0	54.0	7.5	0.4	35.3	79.7	115
	Grabouw	Experiment 2	CEWS	83.6	27.1	8.2	0.7	6.9	7.8	14.7
			PP	72.0	44.3	9.0	0.4	14.2	15.3	29.5
Summer	Mooketsi	Experiment 3	CEWS	79.7	38.0	2.9	0.6	10.0	16.3	26.3
			PP	61.3	47.2	31.2	0.3	14.0	52.1	66.1
	Loskop	Experiment 4	CEWS	81.8	35.0	1.3	0.6	7.8	14.1	21.9
			PP	72.9	49.1	5.2	0.5	14.9	16.4	31.3
All year round	Patensie	Experiment 5	CEWS	82.9	32.8	1.4	0.7	9.2	11.4	20.6
			PP	69.9	45.0	16.5	0.4	13.0	27.8	40.8
		Mean	CEWS	82.0	32.9	3.3	0.7	11.2	13.9	25.0
		Standard deviation		1.4	3.6	2.5	0.05	5.6	4.0	9.1
		Mean	PP	69.0	47.9	13.9	0.4	18.3	38.3	56.5
		Standard deviation		4.1	3.5	9.5	0.06	8.5	24.6	32.0

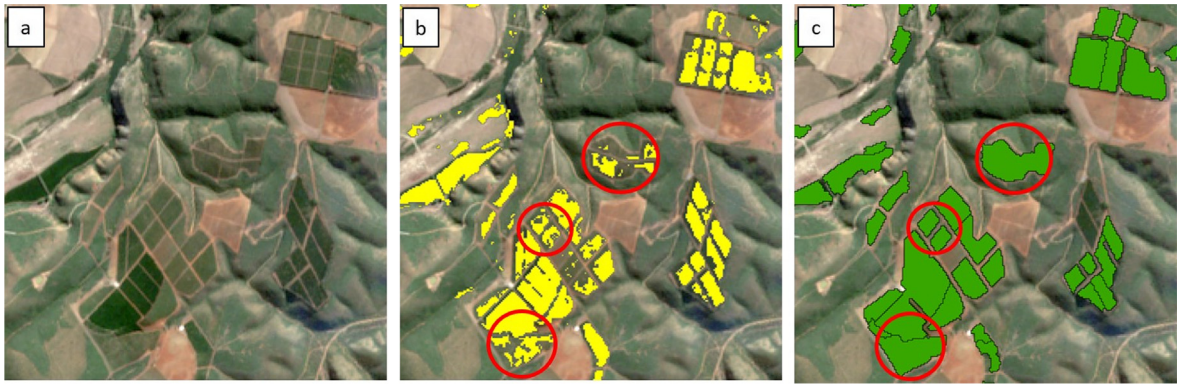

Fig. 3. Cultivated field extraction results for an area in Patensie showing an (a) RBG composite of Sentinel-2 imagery acquired in June 2017, along with the (b) PP and (c) CEWS outputs.

allow agricultural statistics to be calculated per-field, which is highly beneficial in agricultural monitoring systems.

The low standard deviations of the CEWS outputs suggest consistency across different agricultural landscapes. However, some patterns in accuracy were observed. Lower accuracies were noted in areas made up of largely annual rain-fed crops. Waldner et al. (2017) found that annual precipitation and field density were important factors in cropland identification. These factors were also the likely drivers of the lower accuracies (Table 4) recorded in Swartland and Mooketsi, as both sites have relatively low annual precipitation (Table 1). The fields in both sites are also generally irregular in shape and the same crops are often grown in adjacent fields, with minimal separating features (e.g. roads or hedges) that can be utilized by the segmentation algorithm. Thus, some fields were not effectively delineated or identified (Fig. 5). In contrast, higher accuracies were recorded in areas containing predominantly irrigated or perennial crops. For instance, both Loskop and Grabouw have high levels of annual precipitation and more defined boundaries (e.g. roads or hedges) and were thus more easily identified and delineated.

A major advantage of CEWS is that the requirement for training data (of supervised classification) was circumvented by implementing a knowledge-based (ruleset) technique for excluding non-cultivated areas. The collection of training samples relies on human interpretation, making the process time-consuming, expensive and difficult to apply on a large scale (Thenkabail and Wu, 2012). In addition, samples will likely have to be collected for each season due to the dynamic nature of crops (e.g. crop rotations), thus making a supervised approach impractical in the context of operational systems. CART's selection of the maximum NDVI feature for the decision trees of all three of the rainfall regimes suggests that it is a robust multi-temporal variable for discriminating agricultural fields from other land covers across varying climatic regions. This agrees with Waldner et al. (2017), who found that maximum NDVI was the most important variable in developing a national cropland map for South Africa. In contrast, Lambert et al. (2016) found that minimum NDVI was more important for cultivated field identification. Our findings support those of Jia et al. (2014) who also noted the benefits of using multi-temporal NDVI features (maximum, minimum and standard deviation) for land cover differentiation (including cultivated fields). They also found that higher temporal resolution imagery improved the efficiency of the NDVI features. The use of atmospherically corrected level-2A imagery (instead of the TOA reflectance level-1C imagery used in this study) would likely lead to improved and more robust (consistent) classifications and should be employed in future implementations of the proposed methodology.

Our results show that multi-temporal Sentinel-2 imagery can be used to identify and delineate agricultural field boundaries using an OBIA approach. The relatively high temporal frequency (five days) of the imagery allowed for a large number of observations spanning an entire year (e.g. 58 observation dates for the Swartland site). This relatively high temporal frequency increases the chance of cloud-free observations during the growing season. However, the manual selection of cloud-free imagery (as undertaken in this study) should be avoided and an automated technique, such as image compositing, should rather be used for operational implementations. Regarding the spatial resolution of the Sentinel-2 imagery used, the 10 m resolution was sufficient in most cases, but was less effective in areas containing small and irregularly shaped fields (such as those in the Grabouw and Mooketsi study sites). A potential advantage of Sentinel-2 imagery, compared to other EO satellites (e.g. Landsat-8, SPOT-6/7 and RapidEye) is the higher spectral resolution (number of available bands). However, while the red-edge and SWIR bands could potentially aid in the better discrimination between agricultural land covers (e.g. crop type classification), their use for agricultural field boundary delineation is of less value as their spatial resolutions are significantly lower (20–60 m)

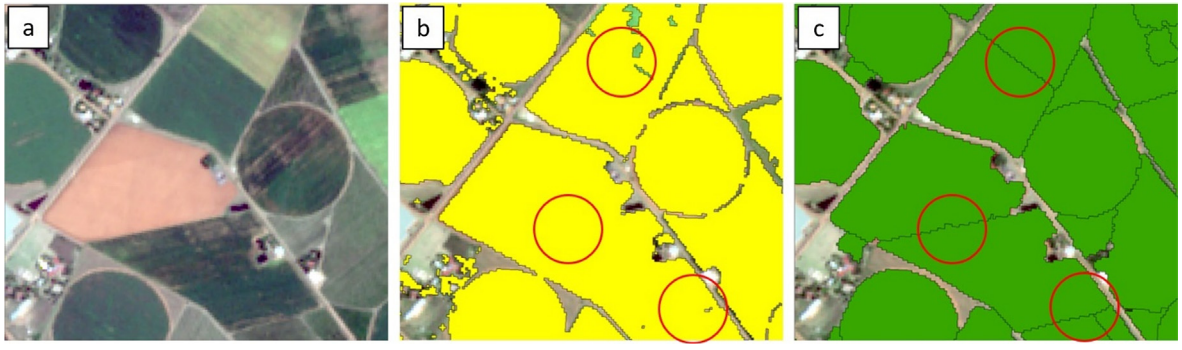

Fig. 4. Cultivated field extraction results for an area in Loskop displaying an (a) RGB composite of Sentinel-2 imagery acquired in January 2018, compared to the (b) PP and (c) CEWS outputs.

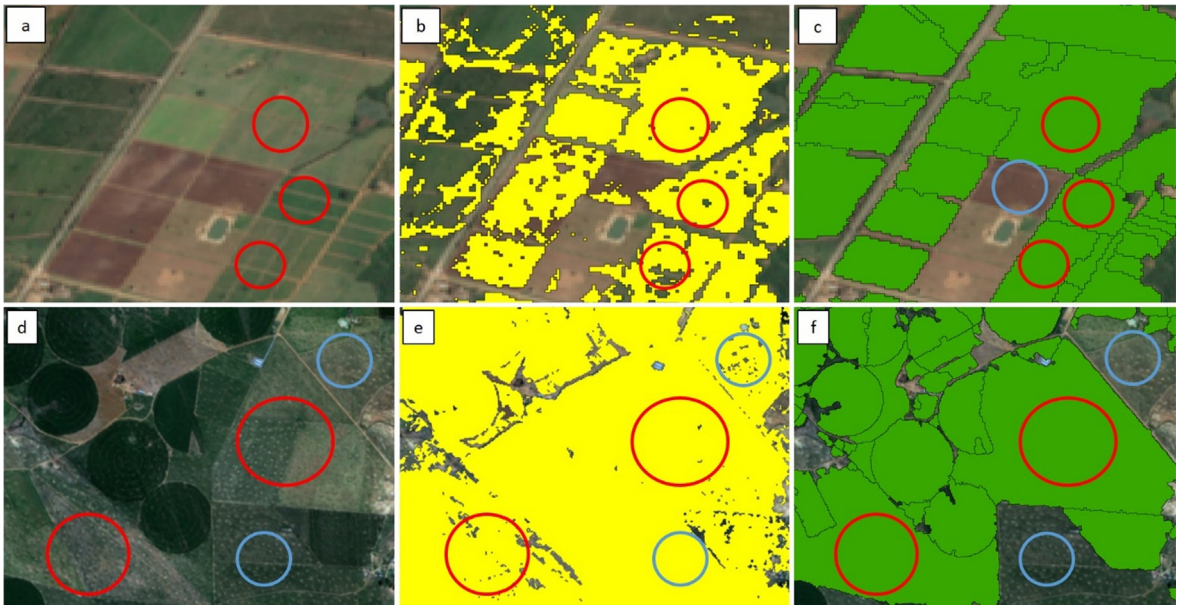

Fig. 5. Cultivated field extraction results for an area in Mooketsi (a – c) and Swartland (d – f) displaying an (a) RGB composite of Sentinel-2 imagery acquired in March 2018, as well as the related (b) PP and (c) CEWS outputs; and (d) an RGB composite of Sentinel-2 imagery acquired during August 2017, accompanied by (e) the PP and (f) CEWS results. The highlighted areas show where both methods failed to identify field boundaries due to low contrast between fields.

(Valero et al., 2016). This observation is in agreement with Immitzer et al. (2016) who mapped crop and tree species in Central Europe using single date Sentinel-2 imagery. They noted a potential limitation of the spatial resolution of Sentinel-2 imagery (particularly the 20 m bands) to map highly fragmented landscapes. A potential solution would be to incorporate VHR imagery (e.g. SPOT 6/7, WorldView 2/3) into the edge detection phase to enhance the field boundaries more finely. This could prove to be advantageous for areas with high homogeneity between fields (e.g. Swartland). It is likely that a single VHR image might be sufficient for identifying permanent field divisions (e.g. hedges or narrow roads), but more work is needed to investigate such an approach.

The five sites selected in this study covered a range of agricultural landscapes with varying environmental conditions. Although the evaluated automated OBIA methodology showed great promise for agricultural field boundary delineation under diverse conditions, it is still unclear whether the developed methodology will perform consistently well when applied to a larger (e.g. national) scale. It is recommended that the modified CEWS is implemented in an operational workflow and evaluated at national or at least regional (provincial) levels.

5. Conclusion

This study evaluated the robustness of a modified OBIA method, called CEWS, to identify and delineate agricultural fields in five agricultural landscapes. The original CEWS method was only implemented in a single, relatively small area with similar conditions, thus an evaluation and subsequent modification was required to test its efficacy in different agricultural and environmental conditions. The CEWS technique was modified in this study and was implemented to delineate agricultural field boundaries in five very diverse agricultural landscapes. A supervised per-pixel classification was performed to serve as a benchmark for comparison purposes. The key findings of the study are:

1. Compared to the supervised per-pixel approach, the knowledge-based CEWS method provided statistically significant and superior results when delineating agricultural fields;
2. The spatial resolution (10 m) of Sentinel-2 imagery is well suited to field boundary delineation in most cases; however, it is less effective in regions containing small and irregular fields;
3. The high temporal resolution (five-day interval) of Sentinel-2 imagery can adequately represent crop phenology throughout the growing season (at least in the selected sites representing South African conditions); and
4. The robustness and transferability of the region-specific rule-sets for excluding uncultivated areas are very encouraging and suggest that an automated knowledge-based approach is feasible for incorporation into an operational multi-temporal OBIA workflow to delineate agricultural fields.

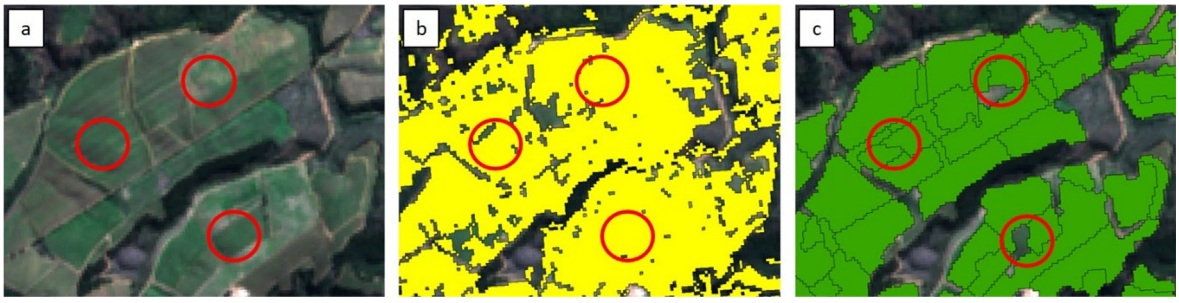

Fig. 6. Cultivated area feature extraction results for an area in Grabouw showing an (a) RGB composite of Sentinel-2 imagery acquired during September 2017, compared to the (b) PP and (c) CEWS outputs. The highlighted areas show where both methods struggled to accurately delineate small and irregularly shaped fields.

ARTICLE IN PRESS

Given the results obtained in this study, the modified CEWS methodology shows great potential for automatically delineating agricultural field boundaries at regional scales. CEWS is recommended for integration into an operational workflow. It is suggested that further research is conducted in which the workflow is applied to a larger scale (i.e. regional or national). The resulting field boundaries can subsequently be integrated into agricultural monitoring systems and aid in the implementation of precision agriculture, crop yield estimates and resource planning.

Declaration of Competing Interest

The authors declare that they have no known competing financial interests or personal relationships that could have appeared to influence the work reported in this paper.

Acknowledgements

This work forms part of a larger project titled “Salt Accumulation and Waterlogging Monitoring System (SAWMS) Development” which was initiated and funded by the Water Research Commission (WRC) of South Africa (contract number K5/2558//4). More information about this project is available in the 2016/2017 WRC Knowledge Review (ISBN 978-1-4312-0912-5) available at www.wrc.org.za. The authors would also like to thank the Centre for Geographical Analysis for providing the Sentinel-2 data, and the National Research Foundation (grant number 106739) for their funding of this project.

References

Alemu, M.M., 2016. Automated farm field delineation and crop row detection from satellite images. University of Twente. [online]. Available from: http://www.itc.nl/library/papers_2016/msc/gfm/alemu.pdf.

Atzberger, C., 2013. Advances in remote sensing of agriculture: Context description, existing operational monitoring systems and major information needs. Remote Sensing 5 (2), 949–981.

Belgiu, M., Csillik, O., 2018. Sentinel-2 cropland mapping using pixel-based and object-based time-weighted dynamic time warping analysis. Remote Sensing of Environment 204, 509–523. https://doi.org/10.1016/j.rse.2017.10.005. November 2017, [online]. Available from:.

Blaschke, T., 2010. Object based image analysis for remote sensing. ISPRS J. Photogrammetry Remote Sensing 65 (1), 2–16. https://doi.org/10.1016/j.isprsjprs.2009.06.004.

Blaschke, T., Lang, S., Lorup, E., Strobl, J., Zeil, P., 2000. Object-oriented image processing in an integrated GIS / remote sensing environment and perspectives for environmental applications. Environ. Inf. Planning, Politics Public 1995, 555–570.

Bontemps, S., Arias, M., Cara, C., Dedieu, G., Guzzonato, E., Hagolle, O., Inglada, J., Matton, N., Morin, D., Popescu, R., Rabaute, T., Savinaud, M., Sepulcre, G., Valero, S., Ahmad, I., Bégué, A., Wu, B., de Abelleyra, D., Diarra, A., Dupuy, S., French, A., Akhtar, I.ul H, Kussul, N., Lebourgeois, V., Page, M. Le, Newby, T., Savin, I., Verón, S.R., Koetz, B., Defourny, P., 2015. Building a data set over 12 globally distributed sites to support the development of agriculture monitoring applications with Sentinel-2. Remote Sensing 7 (12), 16062–16090.

Butenuth, M., Straub, B., Heipke, C., 2004. Automatic Extraction of Field Boundaries from Aerial Imagery. KDNet Symposium on Knowledge-Based Services for the Public Sector, pp. 14–25.

Chen, B., Qiu, F., Wu, B., Du, H., 2015. Image segmentation based on constrained spectral variance difference and edge penalty. Remote Sensing 7 (5), 5980–6004.

Clinton, N., Holt, A., Scarborough, J., Yan, L., Gong, P., 2010. Accuracy assessment measures for object-based image segmentation goodness. Photogramm. Eng. Remote Sens. 76 (3), 289–299.

Delves, L., Wilkinson, R., Oliver, C., White, R., 1992. Comparing the performance of SAR image segmentation algorithms. Int. J. Remote Sens. 13 (11), 2121–2149.

Duro, D.C., Franklin, S.E., Dube, M.G., 2012. A comparison of pixel-based and object-based image analysis with selected machine learning algorithms for the classification of agricultural landscapes using SPOT-5 HRG imagery. Remote Sens. Environ. 118, 259–272. https://doi.org/10.1016/j.rse.2011.11.020. [online]. Available from:.

Duveiller, G., Defourny, P., 2010. A conceptual framework to define the spatial resolution requirements for agricultural monitoring using remote sensing. Remote Sensing Environ. 114 (11), 2637–2650. https://doi.org/10.1016/j.rse.2010.06.001.

Esfahani ALIG, 2014. Delineation of Agricultural Field Boundaries Using Random Sets. University of Twente.

Fan, J., Yau, D.K.Y., Elmagarmid, A.K., Aref, W.G., 2001. Automatic image segmentation by integrating color-edge extraction and seeded region growing. IEEE Trans. Image Process. 10 (10), 1454–1466.

Forkuor, G., Conrad, C., Thiel, M., Zoungrana, B.J.B., Tondoh, J.E., 2017. Multiscale remote sensing to map the spatial distribution and extent of cropland in the sudanian savanna of West Africa. Remote Sensing 9 (8), 1–24.

Fritz, S., See, L., Mccallum, I., You, L., Bun, A., Moltchanova, E., Duerauer, M., Albrecht, F., Schill, C., Perger, C., Havlik, P., Mosnier, A., Thornton, P., Wood-Sichra, U., Herrero, M., Becker-Reshef, I., Justice, C., Hansen, M., Gong, P., Abdel Aziz, S., Cipriani, A., Cumani, R., Cecchi, G., Conchedda, G., Ferreira, S., Gomez, A., Haffani, M., Kayitakire, F., Malanding, J., Mueller, R., Newby, T., Nonguierma, A., Olusegun, A., Ortner, S., Rajak, D.R., Rocha, J., Schepaschenko, D., Schepaschenko, M., Terekhov, A., Tiangwa, A., Vancutsem, C., Vintrou, E., Wenbin, W., van der Velde, M., Dunwoody, A., Kraxner, F., Obersteiner, M., 2015. Mapping global cropland and field size. Glob. Change Biol. 21 (5), 1980–1992.

Huete, A.R., 1988. A soil-adjusted vegetation index (SAVI). Remote Sens. Environ. 25 (3), 295–309.

Immitzer, M., Vuolo, F., Atzberger, C., 2016. First experience with Sentinel-2 data for crop and tree species classifications in central Europe. Remote Sensing 8, 3.

Inglada, J., Arias, M., Tardy, B., Hagolle, O., Valero, S., Morin, D., Dedieu, G., Sepulcre, G., Bontemps, S., Defourny, P., Koetz, B., 2015. Assessment of an operational system for crop type map production using high temporal and spatial resolution satellite optical imagery. Remote Sensing 7 (9), 12356–12379.

Jia, K., Liang, S., Zhang, N., Wei, X., Gu, X., Zhao, X., Yao, Y., Xie, X., 2014. Land cover classification of finer resolution remote sensing data integrating temporal features from time series coarser resolution data. ISPRS J. Photogramm. Remote Sens. 93, 49–55. https://doi.org/10.1016/j.isprsjprs.2014.04.004. [online]. Available from:.

Kaganami, H.G., Beiji, Z., 2009. Region-based segmentation versus edge detection. In: IIH-MSP 2009 - 2009 5th International Conference on Intelligent Information Hiding and Multimedia Signal Processing, pp. 1217–1221.

Karamura, E.B., Jogo, W., Rietveld, A., Ochola, D., Staver, C., Tinzaara, W., Karamura, D.A., Kubiriba, J., Weise, S., 2013. Effectiveness of agro-ecological intensification practices in managing pests in smallholder banana systems in East and Central Africa. Acta Hortic. 986, 119–126.

Lambert, M.J., Waldner, F., Defourny, P., 2016. Cropland mapping over Sahelian and Sudanian agrosystems: A Knowledge-based approach using PROBA-V time series at 100-m. Remote Sensing 8, 3.

Lebourgeois, V., Dupuy, S., Vintrou, É., Ameline, M., Butler, S., Bégué, A., 2017. A combined random forest and OBIA classification scheme for mapping smallholder agriculture at different nomenclature levels using multisource data (simulated Sentinel-2 time series, VHRS and DEM). Remote Sensing 9 (3), 1–20.

Li, D., Zhang, G., Wu, Z., Yi, L., 2010. An edge embedded marker-based watershed algorithm for high spatial resolution remote sensing image segmentation. IEEE Trans. Image Process. 19 (10), 2781–2787.

Lucas, R., Rowlands, A., Brown, A., Keyworth, S., Bunting, P., 2007. Rule-based classification of multi-temporal satellite imagery for habitat and agricultural land cover mapping. ISPRS J. Photogramm. Remote Sens. 62 (3), 165–185.

Lunetta, R.S., Shao, Y., Ediriwickrema, J., Lyon, J.G., 2010. Monitoring agricultural cropping patterns across the Laurentian Great Lakes Basin using MODIS-NDVI data. Int. J. Appl. Earth Obs. Geoinf. 12 (2), 81–88. https://doi.org/10.1016/j.jag.2009.11.005. [online]. Available from:.

Maselli, F., Rembold, F., 2001. Analysis of GAC NDVI Data for Cropland Identification and Yield Forecasting in Mediterranean African Countries, May: 593–602.

Matton, N., Canto, G.S., Waldner, F., Valero, S., Morin, D., Inglada, J., Arias, M., Bontemps, S., Koetz, B., Defourny, P., 2015a. An automated method for annual cropland mapping along the season for various globally-distributed agrosystems using high spatial and temporal resolution time series. Remote Sensing 7 (10), 13208–13232.

Matton, N., Sepulcre Canto, G., Waldner, F., Valero, S., Morin, D., Inglada, J., Aria, M., Bontemps, S., Koetz, B., Defourny, P., 2015b. An Automated method for annual cropland mapping along the season for various globally-distributed agrosystems using high spatial and temporal resolution time series. Remote Sensing 7, 13208–13232.

Meyer, H.P., Niekerk, A. Van, 2015. Assessing Edge and Area Metrics for Image Segmentation Parameter Tuning and Evaluation.

Möller, M., Lymburner, L., Volk, M., 2007. The comparison index: A tool for assessing the accuracy of image segmentation. Int. J. Appl. Earth Obs. Geoinf. 9 (3), 311–321.

Mueller, M., Segl, K., Kaufmann, H., 2004. Edge- and region-based segmentation technique for the extraction of large, man-made objects in high-resolution satellite imagery. Pattern Recogn. 37 (8), 1619–1628.

Ozdogan, M., Yang, Y., Allez, G., Cervantes, C., 2010. Remote sensing of irrigated agriculture: Opportunities and challenges. Remote Sensing 2 (9), 2274–2304.

Peña, J., Gutiérrez, P., Hervás-Martínez, C., Six, J., Plant, R., López-Granados, F., 2014. Object-based image classification of summer crops with machine learning methods. Remote Sensing 6 (6), 5019–5041 [online]. Available from: http://www.mdpi.com/2072-4292/6/6/5019/.

Pittman, K., Hansen, M.C., Becker-Reshef, I., Potapov, P.V., Justice, C.O., 2010. Estimating global cropland extent with multi-year MODIS data. Remote Sensing 2 (7), 1844–1863.

Quynh Trang, N.T., Toan, L.Q., Huyen Ai, T.T., Vu Giang, N., Viet Hoa, P., 2016. Object-based vs. pixel-based classification of mangrove forest mapping in Vien An Dong Commune, Ngoc Hien District, Ca Mau Province Using VNREDSat-1 Images. Adv. Remote Sensing 05, 04: 284–295. [online]. Available from: http://www.scirp.org/journal/doi.aspx?DOI=10.4236/ars.2016.54022.

Ramadevi, Y., Sridevi, T., Poornima, B., Kalyani, B., 2010. Segmentation and object recognition using edge detection techniques. Int. J. Comput. Sci. Inf. Technol. 2 (6), 153–161.

Roumenina, E., Atzberger, C., Vassilev, V., Dimitrov, P., Kamenova, I., Banov, M., Filchev, L., Jelev, G., 2015. Single- and multi-date crop identification using PROBA-V 100 and 300 m S1 products on Zlatia Test Site, Bulgaria. Remote Sensing 7 (10),

ARTICLE IN PRESS

13843–13862.
Rydberg, A., Borgefors, G., 1999. Extracting multispectral edges in satellite images over agricultural fields. In: Proceedings - International Conference on Image Analysis and Processing, ICIAP 1999, pp. 786–791.
Rydberg, A., Borgefors, G., 2001. Integrated method for boundary delineation of agricultural fieldsin multispectral satellite images. IEEE Trans. Geosci. Remote Sens. 39 (11), 1678–1680.
Schultz, B., Immitzer, M., Formaggio, A.R., Sanches, I.D.A., Luiz, A.J.B., Atzberger, C., 2015. Self-guided segmentation and classification of multi-temporal Landsat 8 images for crop type mapping in Southeastern Brazil. Remote Sensing 7 (11), 14482–14508.
Thenkabail, P.S., Wu, Z., 2012. An automated cropland classification algorithm (ACCA) for Tajikistan by combining landsat, MODIS, and secondary data. Remote Sensing 4 (10), 2890–2918.
Tollefson, J., 2012. Seven billion and counting. NATURE, 2011. Macmillan Publishers Limited.
Turker, M., Kok, E.H., 2013. Field-based sub-boundary extraction from remote sensing imagery using perceptual grouping. ISPRS J. Photogramm. Remote Sens. 79, 106–121. https://doi.org/10.1016/j.isprsjprs.2013.02.009. [online]. Available from:.
Valero, S., Morin, D., Inglada, J., Sepulcre, G., Arias, M., Hagolle, O., Dedieu, G., Bontemps, S., Defourny, P., Koetz, B., 2016. Production of a dynamic cropland mask by processing remote sensing image series at high temporal and spatial resolutions. Remote Sensing 8 (1), 1–21.
Waldner, F., Hansen, M.C., Potapov, P.V., Löw, F., Newby, T., Ferreira, S., Defourny, P., 2017. National-scale cropland mapping based on spectral-temporal features and outdated land cover information. PLoS ONE 12 (8), 1–25.
Watkins, B., Van Niekerk, A., 2019. A comparison of object-based image analysis approaches for field boundary delineation using multi-temporal Sentinel-2 imagery. Comput. Electron. Agriculture 158, February: 294–302. [online]. Available from: https://doi.org/10.1016/j.compag.2019.02.009.
Weidner, U., 2008. Contribution to the assessment of segmentation quality for remote sensing applications. Int. Arch. Photogrammetry, Remote Sensing Spatial Inf. Sci. 37 (B7), 479–484.
Wuest, B., Zhang, Y., 2009. Region based segmentation of QuickBird multispectral imagery through band ratios and fuzzy comparison. ISPRS J. Photogramm. Remote Sens. 64 (1), 55–64. https://doi.org/10.1016/j.isprsjprs.2008.06.005. [online]. Available from:.
Yan, L., Roy, D.P., 2016. Conterminous United States crop field size quantification from multi-temporal Landsat data. Remote Sens. Environ. 172, 67–86. https://doi.org/10.1016/j.rse.2015.10.034. [online]. Available from:.
Zhan, Q., Molenaar, M., Tempfli, K., Shi, W., 2005. Quality assessment for geo-spatial objects derived from remotely sensed data. Int. J. Remote Sens. 26 (14), 2953–2974.
Zheng, B., Myint, S.W., Thenkabail, P.S., Aggarwal, R.M., 2015. A support vector machine to identify irrigated crop types using time-series Landsat NDVI data. Int. J. Appl. Earth Obs. Geoinf. 34 (1), 103–112. https://doi.org/10.1016/j.jag.2014.07.002. [online]. Available from:.